

---

# BOOSTING MULTIMODAL LARGE LANGUAGE MODELS WITH VISUAL TOKENS WITHDRAWAL FOR RAPID INFERENCE

---

Zhihang Lin<sup>1</sup> Mingbao Lin<sup>2</sup> Luxi Lin<sup>1</sup> Rongrong Ji<sup>1\*</sup>

<sup>1</sup>Key Laboratory of Multimedia Trusted Perception and Efficient Computing,  
Ministry of Education of China, Xiamen University, China. <sup>2</sup>Skywork AI

zhihanglin@stu.xmu.edu.cn, linmb001@outlook.com, lewuluu@gmail.com, rrji@xmu.edu.cn

## ABSTRACT

Multimodal large language models (MLLMs) demand considerable computations for inference due to the extensive parameters and the additional input tokens needed for visual information representation. Herein, we introduce Visual Tokens Withdrawal (VTW), a plug-and-play module to boost MLLMs for rapid inference. Our approach is inspired by two intriguing phenomena we have observed: (1) the attention sink phenomenon that is prevalent in LLMs also persists in MLLMs, suggesting that initial tokens and nearest tokens receive the majority of attention, while middle vision tokens garner minimal attention in deep layers; (2) the presence of information migration, which implies that visual information is transferred to subsequent text tokens within the first few layers of MLLMs. As per our findings, we conclude that vision tokens are not necessary in the deep layers of MLLMs. Thus, we strategically withdraw them at a certain layer, enabling only text tokens to engage in subsequent layers. To pinpoint the ideal layer for vision tokens withdrawal, we initially analyze a limited set of tiny datasets and choose the first layer that meets the Kullback-Leibler divergence criterion. Our VTW approach can cut computational overhead by over 40% across diverse multimodal tasks while maintaining performance. Our code is released at <https://github.com/lzhxmu/VTW>.

**Keywords** Multimodal Large Language Models · Rapid Inference · Vision Tokens Withdrawal

## 1 Introduction

In recent years, major progress has been made in generative AI with the development of large language models (LLMs) [1, 2, 3]. Multimodal large language models (MLLMs) [4, 5, 2, 6] combine vision encoders, like CLIP [7], to extract visual features, enhancing LLM’s reasoning abilities for complex tasks like visual question answering (VQA) [8, 9] and visual reasoning [10, 11, 12]. However, MLLMs entail high inference cost due to their billions of parameters and the quadratic computational increase with the length of the input sequence. Converting a high-resolution image into vision tokens further increase the inference cost [6]. The high inference cost of MLLMs hinders their applicability in real-time scenarios.

Recent methods [15, 16, 17, 14] aim to reduce the computational cost of MLLMs through token reduction. The primary goal is to keep so-called “important” tokens based on predefined metrics and remove or merge the rest. However, these approaches have some shortcomings that need to be addressed. (1) Lack of flexibility. Methods like LLaVA-PruMerge [17] employ identical vision tokens to represent an image for different questions in VQA. However, for datasets like MME, POPE, and AI2D [12, 18, 9], numerous questions are associated with the same image, each focusing on a distinct area of the image, as illustrated in Figure 1(a). Thus, LLaVA-PruMerge cannot dynamically adjust the important tokens based on the questions, leading to a lack of flexibility and a significant accuracy drop of 160.4 on MME [12] benchmark. (2) Incomplete importance metric. Almost all methods necessitate the design of an importance metric for token reduction, such as cross-modal guidance for CrossGET [15] and attention score for FastV [14]. However, there is limited theoretical evidence to establish which importance metric is the most optimal and accurate. A low importance score for a token does not necessarily indicate that the token is unimportant. Moreover,

---

\*Corresponding author

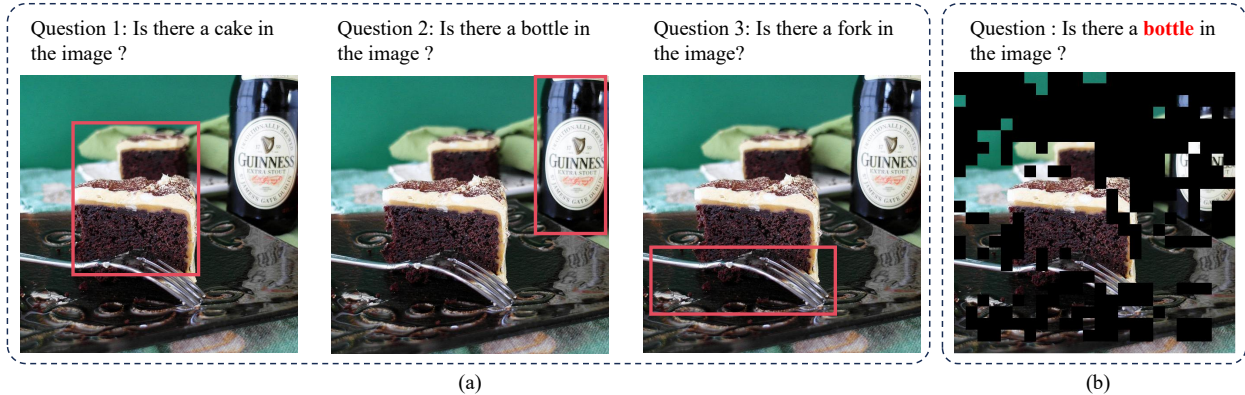


Figure 1: (a) An instance from POPE dataset [13]. The red box represents the key area for answering the corresponding question. (b) The visualization of “important” vision tokens use the important metric from FastV [14]. Some genuinely important tokens like “bottle” are pruned, while less important tokens like “cake” are preserved.

some genuinely important tokens may also be pruned in these methods, as illustrated in Figure 1(b). Thus, designing a comprehensive importance metric to determine which tokens are important is challenging. (3) Incompatibility with KV Cache. KV Cache [13] is an essential approach for speeding up MLLMs decoding by storing prior tokens’ Key and Value states. FastV [14] dynamically prunes partial vision tokens after a particular layer, with retained tokens varying for each auto-regressive prediction. Thus, the cached KV of previous tokens cannot be reused because the retained vision tokens change with each prediction. To use KV Cache to speed up the decoding stage, all KV Cache must be maintained in the initial prediction process. However, this leads to memory occupation for pruned tokens and reduces the memory benefit of token reduction. Therefore, current token reduction methods don’t fully meet the practical acceleration needs of MLLMs for various complex multimodal tasks.

Driven by the above analysis, we recognize that instead of being stuck in figuring out individual solutions to address the above shortcomings, a more comprehensive approach would be to withdraw all vision tokens after a specific layer. In doing so, all vision tokens are preserved within the first few layers of MLLMs, ensuring flexibility across various multi-modal tasks. Second, there is no need to design a comprehensive importance metric for selecting crucial tokens, thus avoiding the unintentional removal of important vision tokens. Third, this approach is compatible with KV Cache because all vision tokens are preserved and removed simultaneously. Inspired by these insights, we conduct a thorough analysis to explore the possibility of removing all vision tokens after a specific layer. In particular, we perform extensive visualizations in Sec. 3.2 and uncover some intriguing phenomena: (1) The attention sink phenomenon in LLMs [19] persists in MLLMs, where initial and nearest tokens gain the most attention, while middle vision tokens receive minimal attention. (2) As the number of generated tokens increases, vision tokens receive less attention, while text tokens garner more attention. These results are attributed to the causal self-attention operation in LLMs, which only allows tokens to attend to preceding tokens, ensuring the model’s generation depends on preceding content. As a consequence of this operation, information from visual tokens migrates to subsequent text tokens through several layers of attention transformation. Therefore, the latest token tends to pay progressively less attention to vision tokens and more attention to text tokens in the deeper layers and when there are more and more generated text tokens.

In this paper, we attempt to boost multimodal large language models with Visual Tokens Withdrawal (VTW) strategy for rapid inference. Given that vision tokens become less crucial in deep layers of LLMs and their information has already been absorbed by the subsequent text tokens, we propose withdrawing them in the deep layers. VTM implements a visual tokens withdrawal approach at a specific layer of MLLMs, as illustrated in Figure 2. Before this layer, computations proceed as usual; after this layer, vision tokens are removed, and only text tokens continue to participate the computation of deep layers. To determine the withdrawal layer, we first sample a small subset of datasets. Then, we calculate the Kullback-Leibler divergence between the output logits of the standard decoding and the visual tokens withdrawal decoding in each layer. Finally, we select the first layer that meets the Kullback-Leibler divergence criterion as vision token withdrawal layer.

We carry out extensive experiments on various multimodal tasks, such as visual question answering [9, 8], hallucination evaluation [18], and visual reasoning [10, 12], to show the efficacy of our VTW. Notably, VTW can reduce over 40% FLOPs on AI2D [9], SQA\_image [8], MMMU\_Val [10], MMB\_EN [11], POPE [18], and MME [12] without compromising performance. Also, VTW is applicable to the multimodal chatbot [4] to achieve accelerated inference with imperceptible differences in the answers.

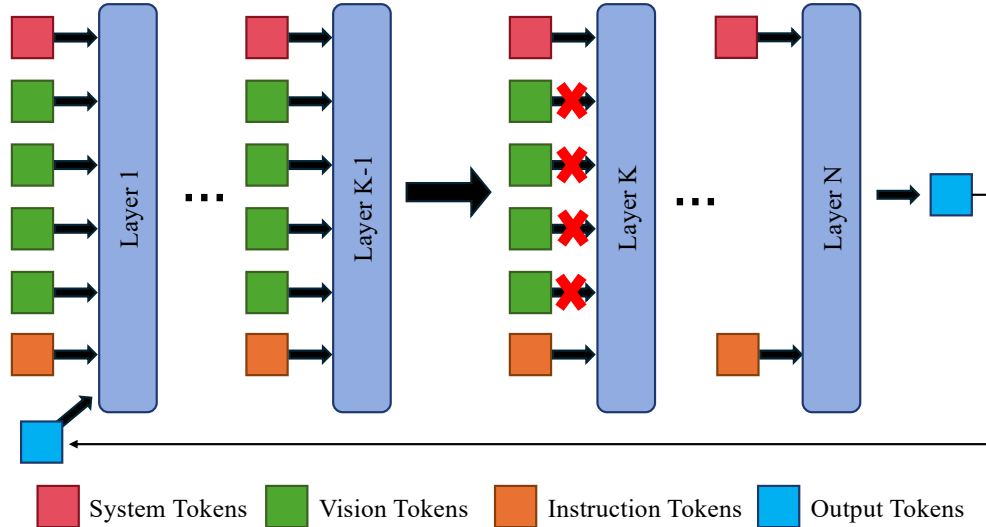


Figure 2: The framework of our method. Vision tokens are withdrawn in the  $K$ -th layer of multimodal large language models.

## 2 Related Work

### 2.1 Multimodal Large Language Models

Large Language Models (LLMs) such as GPT series [20, 1], Gemini series [2], and LLaMA series [3, 21] have revolutionized the field of natural language processing (NLP). Recently, these LLMs have been enhanced with multimodal perception and understanding capabilities, including image [4, 22, 5], video [23], audio processing [24], *etc.* LLaVA [4, 25] combines the visual encoder of CLIP [7] with the language decoder LLaMA [4] and fine-tunes them on instruction-following datasets, creating a versatile visual assistant. BLIP-2 [5] ingeniously bridges the gap between a static image encoder and a frozen LLM by introducing a trainable Q-Former, thereby achieving remarkable zero-shot image-to-text generation capability. Video-LLaMA [26] further augments LLMs by incorporating video and audio understanding through a multi-branch cross-modal pre-training framework, which aligns vision-language and audio-language. Nevertheless, these MLLMs introduce a substantial number of additional tokens when integrating information from other modalities. For example, LLaVA [4] employs 576 vision tokens to represent an image of resolution  $336 \times 336$ , and this number escalates for higher-resolution images. The problem is even more significant in Video-LLaMA [26] and LLaVA-NeXT [6], which greatly increase the number of input tokens for MLLMs. Despite their excellent performance, the computational cost of MLLMs, proportional to the square of input tokens, is a major hurdle. This high cost hinders their use in real-world situations.

### 2.2 Vision Token Reduction

Token pruning [27, 28, 29] and merging [30, 31] techniques directly reduce the number of tokens, thereby decreasing the inference time and memory usage of transformers. In vision transformers [32], EViT [29] and Evo-ViT [28] fuse non-critical tokens into a single token for token reduction. ToMe [30] employs a binary soft-matching algorithm to merge redundant tokens, while Token Pooling [31] utilizes a clustering algorithm for token merging. DiffRate [33] and PPT [34] further integrate both token pruning and merging into a unified framework to dynamically reduce redundant tokens. In NLP, PoWER-BERT [35] selectively eliminates redundant tokens based on word vector similarity, thereby enhancing inference speed. LTP [36] learns layer-specific thresholds using differentiable soft binarization masks and compares token importance scores to these thresholds to prune unimportant tokens. In MLLMs, CrossGET [15] and MADTP [16] introduce special tokens to align tokens of different modalities and use these special tokens to guide token pruning/merging, extending token reduction to multi-modality. LLaVA-PruMerge [17] leverages the spatial redundancy in vision tokens and proposes a token reduction module that employs the similarity between the class token and spatial tokens as a key criterion for pruning and merging vision tokens. Chen *et al.* [14] found that most image tokens receive inefficient attention after the second decoder layer, and pruned half of the image tokens without sacrificing performance. Instead of pruning/merging partial image tokens, we propose eliminating all image tokens at an intermediate layer.

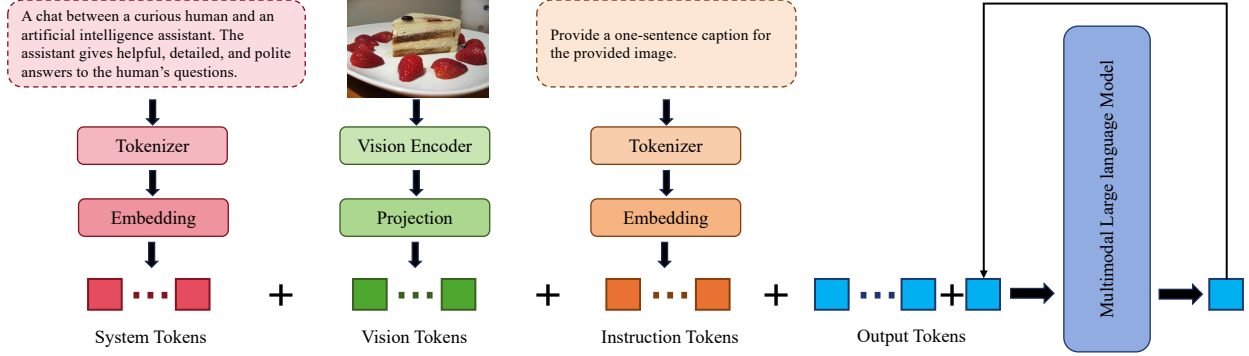


Figure 3: The illustration for the input of a multimodal large language model. The input tokens are composed of system tokens, vision tokens, instruction tokens, and output tokens.

### 3 Methodology

#### 3.1 Motivations

Multimodal large language models (MLLMs) typically comprise a pre-trained vision encoder, a cross-modal projector, and a pre-trained large language model (LLM). Herein, we utilize LLaVA [4], a recent SOTA method, to illustrate the architecture of MLLMs.

The vision encoder, such as CLIP ViT-L [7], is employed to extract visual features from an input image. These visual features are represented as a set of token sequences, referred to as vision tokens. Subsequently, a cross-modal projector transforms these vision tokens into the text embedding space, thereby aligning the outputs of the vision encoder with the LLM. The core of MLLMs is a pre-trained LLM, such as Vicuna [37], which is tasked with understanding the multimodal context and providing an appropriate response. The integration of these components enables MLLMs to effectively process and interpret both textual and visual data, providing a comprehensive understanding of the inputs.

MLLMs require significant computational resources for inference, with the bulk of the computation being attributed to the LLM, given that the size of the visual encoder, such as ViT-L (0.3B), is typically much smaller in comparison to the LLM, such as Vicuna (7B or 13B). In MLLMs, the main computational complexity for a decoder layer comes from multi-head attention (MHA) and feed-forward network (FFN). Assuming the input sequence length is  $s$ , hidden embedding size is  $h$ , and the FFN up-scaling factor is 4, the computational complexity for a transformer decoder layer is [38, 33, 14]:

$$\Omega(MHA + FFN) = 2s^2h + 12sh^2, \quad (1)$$

where computational complexity is quadratically influenced by the input length  $s$ . Therefore, efficient token management is crucial for optimizing the efficiency of MLLMs.

The input tokens of LLaVA, as illustrated in Figure 3, consist of system tokens, vision tokens, instruction tokens, and output tokens. The system tokens are derived from fixed system prompts, which establish a dialogue system for LLaVA during both training and inference stages. Meanwhile, the instruction tokens originate from user, which specify the query question for the given image. As shown in Figure 3, LLaVA preprocesses the input from various modalities and then concatenates all these tokens to form the inference input as:

$$X_1^t = [S_1, \mathcal{V}_1, I_1, O_1^t] \quad (2)$$

where  $X_i^t$  denotes inputs of the  $i$ -th layer in  $t$ -th inference.  $S_1$ ,  $\mathcal{V}_1$ , and  $I_1$  denote system tokens, vision tokens, and instruction tokens, while  $O_1^t$  denotes output tokens at the  $t$ -th inference and  $O_1^0 = \phi$ .

In LLaVA, there are 576 vision tokens and 35 system tokens. The quantity of instruction tokens varies depending on user instructions and is generally fewer than the number of vision tokens. According to Eq. (1), the vision tokens account for the majority of the computation in the inference process, as they constitute most of the input tokens. Recent works [14, 17] have attempted to reduce computation by decreasing the number of vision tokens. However, these methods suffer from limited flexibility, incomplete importance metric, and incompatibility with KV Cache, as elaborated in Sec. 1. Addressing these issues remains an open challenge.

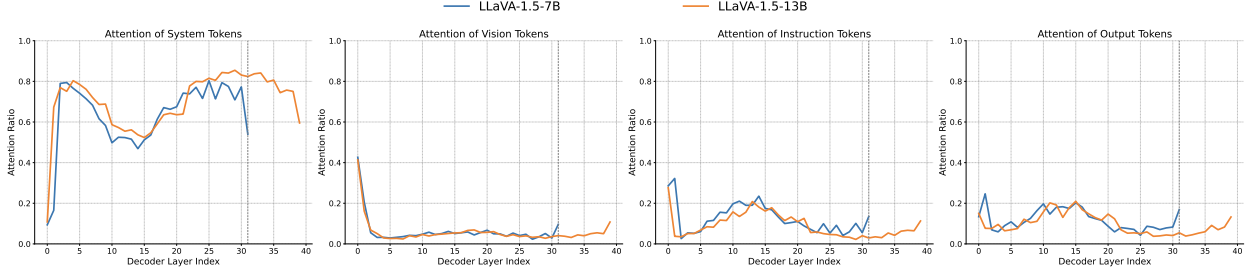


Figure 4: The output token’s attention towards various input token types across different layers. Our visualizations are conducted on a combined subset of AI2D [9], MMMU\_Val [10], MME [12], and POPE [13], utilizing LLaVA-1.5-7B [4] and LLaVA-1.5-13B [4] models (100 samples from each dataset). The attention values are averaged across all attention heads and output tokens.

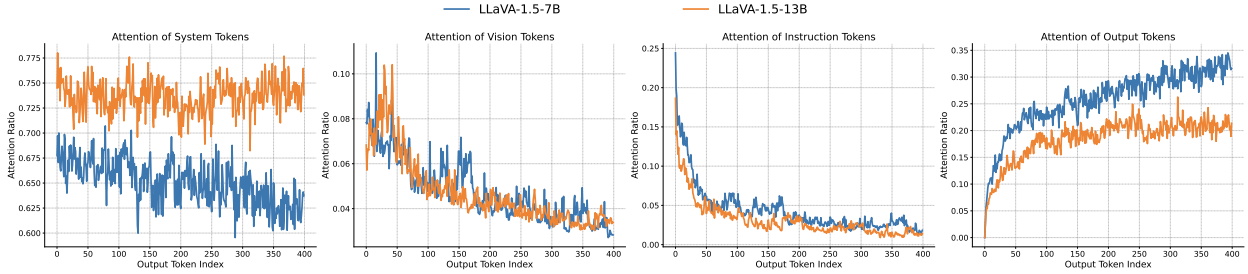


Figure 5: The output token’s attention towards various input token types across output tokens. Our visualization is conducted on a subset of AI2D [9], MMMU\_Val [10], MME [12], and POPE [13] (20 samples from each dataset), utilizing LLaVA-1.5-13B [4]. The attention is averaged across all attention heads and layers.

### 3.2 Unnecessity of Vision Tokens in Deep Layers of MLLMs

Given that input tokens  $X_i^t$  consist of various types of tokens, it is natural to question whether the contribution of each token type to the prediction of the output token is equal or is proportional to their size. Inspired by StreamingLLM [19], we opt for attention scores as the evaluation metrics. Specifically, attention scores are derived from the causal self-attention operation within a decoder layer in LLMs. In the  $i$ -th causal self-attention layer, the hidden feature  $X_i^t$  is transformed into queries  $Q_i^t$ , keys  $K_i^t$ , and values  $V_i^t$  using three distinct learnable projection matrices. Consequently, the causal self-attention, abbreviated as CSA, can be expressed as:

$$CSA(Q_i^t, K_i^t, V_i^t) = A_i^t \cdot V_i^t, \tag{3}$$

where causal attention map  $A_i^t = \text{Softmax}(\frac{Q_i^t K_i^{tT} + \Lambda}{\sqrt{d}})$  and  $d$  is the hidden size of LLM.  $\Lambda$  is an upper triangular matrix where all non-zero elements are set to  $-\infty$ , and the diagonal elements are set to 0. Here, for simplicity, we omit the expression of multi-head causal self-attention. We select the last row of  $A_i^t$  as the attention score  $\alpha_i^t$ , considering that only the final token is utilized to predict the output token in an auto-regressive manner. Based on the positions of system tokens, vision tokens, instruction tokens, and output tokens, we categorize  $\alpha_i^t$  into  $\alpha_i^{t,sys}$ ,  $\alpha_i^{t,vis}$ ,  $\alpha_i^{t,ins}$ , and  $\alpha_i^{t,out}$ . Then, we aggregate the attention scores of each input type, resulting  $\beta_i^{t,sys}$ ,  $\beta_i^{t,vis}$ ,  $\beta_i^{t,ins}$ , and  $\beta_i^{t,out}$ . These variables denote the contributions of each input type to the output prediction.

We visualize  $\beta$  towards various input token types across different layers in Figure 4 and across different output tokens in Figure 5. Two intriguing phenomena can be found: (1) In the initial layers of LLaVA, the attention allocated to system tokens significantly increases, while the attention directed towards vision tokens considerably decreases. In the middle and deep layers, the attention received by all 576 vision tokens amounts to a mere 5%, while the attention towards 35 system tokens can reach 80% or higher. (2) As the quantity of generated tokens grows, vision tokens attract less attention, whereas output tokens gain increased attention.

Utilizing the “attention sink” concept from LLM [19], we explain the fluctuating attention towards system tokens in the shallow and deep layers of LLMs. In the first few layers, the output token interacts with all other tokens through causal self-attention to accumulate semantic information. Consequently, the attention directed towards system tokens is minimal due to their limited semantic content. In the deep layers, the output token possesses sufficient self-contained

Table 1: The ablation study of LLaVA-1.5-7B on MME [12] under various experimental settings. In both (b) and (c), we remove vision tokens in the 16-th layer of LLaVA-1.5-7b. “non-content” denotes a misleading image full of white area.

Experimental Setting	Score
LLaVA-1.5-7B	1866.10
(a) w/o image	970.89 (-895.21)
(b) w non-content image at 1st–16-th layers	845.39 (-1020.71)
(c) w original image at 1st–16-th layers	1872.43 (+6.33)

information for its prediction. However, owing to the nature of the softmax function, which cannot assign zero attention to undesired tokens, the output token will predominantly focus on tokens with minimal semantic information, such as system tokens, to avoid incorporating undesired information from other tokens.

To explain why instruction tokens and output tokens receive greater attention than vision tokens, we introduce the concept of “information migration.” Owing to causal self-attention, tokens can attend only to preceding tokens. Instruction and output tokens can attend to all vision tokens, while vision tokens cannot attend to instruction tokens or output tokens. After multiple transformations of causal self-attention layers, instruction and output tokens incorporate both visual and textual information, thus attracting more attention from output tokens.

To verify that the information migration is completed within the first few layers of MLLMs, we design ablation studies using LLaVA-1.5-7B on MME, a comprehensive evaluation benchmark for MLLMs. As demonstrated in Table 1, without any visual information, the score of LLaVA-1.5-7B decreases by 895.21, emphasizing the significance of visual information in evaluation. Interestingly, MLLMs can handle certain questions using only textual information, as evidenced by a total score of 970.89. By comparing the results of (a), (b), and (c), we observe that MLLMs achieve comparable results with baseline in the (c) setting since the correct visual information has migrated to the subsequent text tokens before 16-th layer. Besides, (b) yields a lower score than (a), as the misleading visual information has migrated to the subsequent text tokens before 16-th layer. These findings provide compelling evidence that information migration occurs within the first few layers of MLLMs.

Hence, we can conclude that **vision tokens are unnecessary in the deep layers of MLLMs**, as the information from vision tokens has migrated to the subsequent text tokens within the first few layers of MLLMs. Consequently, it is justifiable to eliminate all vision tokens in a particular layer during the inference of MLLMs.

### 3.3 Visual Tokens Withdrawal

In this section, we review the standard inference process of MLLMs, followed by a comprehensive introduction to incorporate visual tokens withdrawal into the MLLMs framework.

Remember that the symbol  $X_i^t$  represents the input of the  $i$ -th layer during the  $t$ -th inference pass of MLLMs, as formulated in Eq. (2). The LLM employs an  $N$ -layer transformer architecture decoder to effectively predict output tokens:

$$\begin{aligned} X_{N+1}^t &= D_{1:N}(X_1^t), \\ X_1^{t+1} &= [X_1^t, P(X_{N+1}^t)], \end{aligned} \quad (4)$$

where  $D_{i:j}(\cdot)$  denote a stack of decoder layers from layer  $i$  to layer  $j$ . The function  $P(\cdot)$  predicts subsequent output tokens and calculate their embeddings by taking hidden features as input.

Keeping in mind that the vision tokens are not necessary in the deep layers of MLLMs due to the information migration, we proceed to withdraw these tokens at the  $K$ -th layer:

$$\begin{aligned} X_K^t &= D_{1:K-1}(X_1^t), \\ \mathcal{X}_K^t &= X_K^t - \mathcal{V}_K^t, \\ \mathcal{X}_{N+1}^t &= D_{K:N}(\mathcal{X}_K^t). \end{aligned} \quad (5)$$

In other words, before reaching the  $K$ -th layer, computations carry on as usual; However, after the  $K$ -th layer, vision tokens are withdrawn, leaving only text tokens to engage in the computation of deep layers, an illustration of which is depicted in Fig. 2.

Given the various variants and architectures of MLLMs, such as LLaVA-1.5-7B/13B [4], LLaVA-NeXT-7B [6], among other, it is important to note that more complex tasks may require additional layers to process vision tokens for accurate

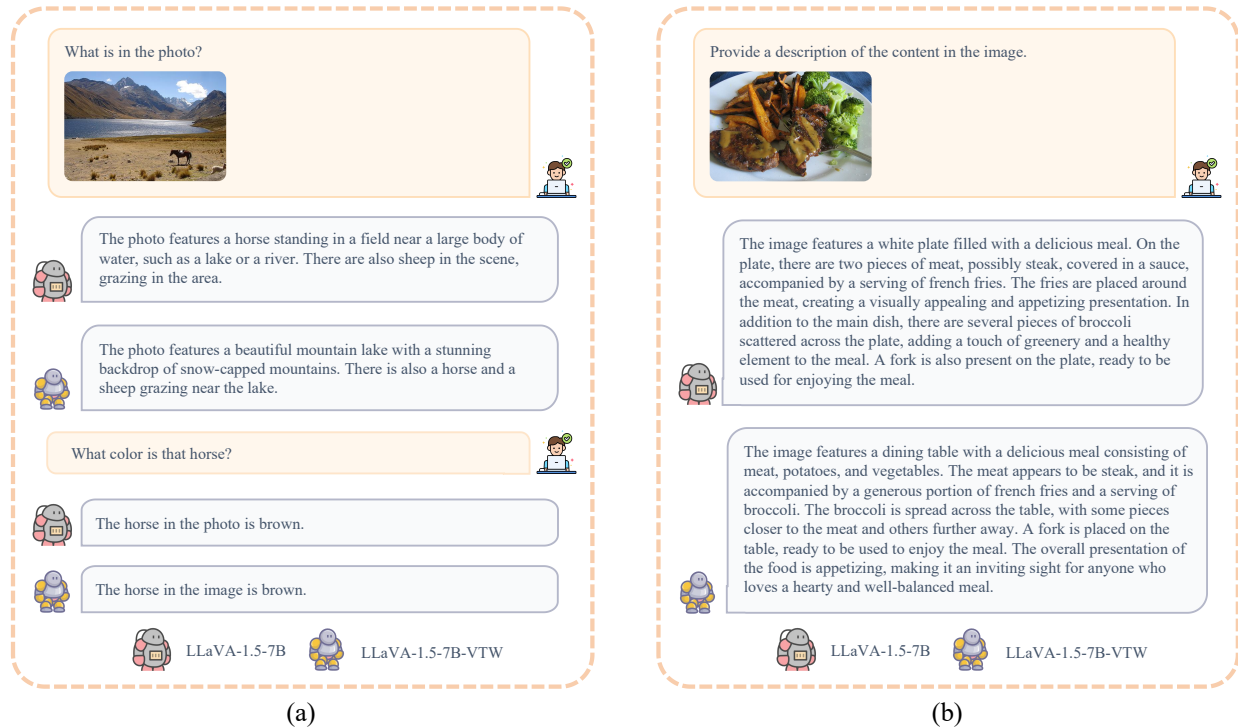


Figure 6: (a) The chatbot dialogue comparison between original LLaVA-1.5-7B [4] and our LLaVA-1.5-7B-VTW. (b) The chatbot dialogue comparison between original LLaVA-1.5-13B [4] and our LLaVA-1.5-7B-VTW.

predictions. Consequently, the optimal withdrawal layer  $K$  varies depending on the specific MLLMs and tasks at hand. To determine the appropriate value for  $K$ , we randomly sample a tiny subset of the target datasets for guidance. From Fig. 4 that vision tokens receive minimal attention after layer 5, we enumerate  $K$  with values ranging from 5 to  $N$ , and compute the Kullback-Leibler divergence between the standard output logits and the VTW’s output logits. We then select the first layer that satisfies the criterion as the withdrawal layer  $K$ :

$$KL(lm_{head}(X_{N+1}), lm_{head}(\mathcal{X}_{N+1})) < \eta, \quad (6)$$

where,  $KL(\cdot)$  represents Kullback-Leibler divergence,  $lm_{head}(\cdot)$  is the project head of LLM,  $X_{N+1}$  and  $\mathcal{X}_{N+1}$  are respectively calculated using Eq. (4) and Eq. (5), and  $\eta$  denotes the threshold.

## 4 Experimentation

### 4.1 Experimental Setting

Our proposed VTW method serves as a seamless extension to off-the-shelf pre-trained MLLMs, requiring no additional training costs. The implementation of VTW merely requires the addition of a few lines of code. In our experiments, we apply VTW to popular open-source MLLMs, such as LLaVA-1.5-7B [4], LLaVA-1.5-13B, and LLaVA-NeXT-7B [6]. LLaVA-NeXT achieves the best performance compared with other open-source MLLMs like CogVLM [39] and Yi-VL [40]. We conduct comprehensive experiments across a multitude of multimodal tasks, such as VQA [9, 8], hallucination evaluation [18], and visual reasoning [12, 10, 11]. We use lmms-eval [41], an evaluation framework, to evaluate MLLMs on different datasets. These experiments are designed to showcase the robustness and generalizability of VTW. In our experiment setup, the tiny subset size was set to 20, and the threshold  $\eta$  was set to 0.003. For the multimodal chatbot, we withdraw vision tokens at the intermediate layers of MLLMs. Specifically, we use the 16-th and 20-th layers for LLaVA-1.5-7B and LLaVA-1.5-13B, respectively.

### 4.2 Multimodal Chatbot

We assess the effectiveness of integrating our VTW into multimodal chatbots. Our main goal is to boost the chatbot’s response speed without compromising response quality. We compare the responses of MLLMs before and after applying VTW in Figure 6. More results have been illustrated in Appendix A. We can see that the chatbots equipped with our

Table 2: Comparison of different training-free methods for accelerating MLLMs inference. SQA\_Image represents the ScienceQA [8] image subset, MMMU\_Val represents the validation subset of MMMU [8], and MMB\_EN denotes the english subset of MMBench [11]. To ensure fair comparison, we manually set the visual tokens withdrawal layer  $K$  as 16 to maintain the FLOPs of VTW lower than that of FastV [14]. We employ **bold** formatting to highlight the best result. We use the average input length on MME to calculate TFLOPs.

Methods	TFLOPs ↓	AI2D ↑	SQA_Image ↑	MMMU_Val ↑	MMB_EN ↑	POPE ↑	MME ↑
LLaVA-1.5-7B	8.48 (100.00%)	55.21	69.61	35.60	64.09	85.83	1866.10
+ FastV	4.91 (57.90%)	55.14	68.96	35.80	<b>64.26</b>	82.49	1864.35
+ VTW (K=16)	<b>4.68</b> (55.19%)	<b>55.44</b>	<b>69.66</b>	<b>36.30</b>	64.00	<b>85.96</b>	<b>1872.43</b>
LLaVA-1.5-13B	16.50 (100.00%)	59.26	72.83	<b>34.90</b>	68.73	<b>86.02</b>	1827.26
+ FastV	9.56 (57.94%)	58.87	<b>73.03</b>	34.60	68.30	85.15	<b>1855.11</b>
+ VTW (K=20)	<b>9.10</b> (55.15%)	<b>59.39</b>	72.88	<b>34.90</b>	<b>68.81</b>	85.93	1828.79
LLaVA-NeXT-7B	28.73 (100.00%)	65.31	<b>70.15</b>	35.30	<b>67.18</b>	<b>86.44</b>	1846.33
+ FastV	15.67 (54.54%)	64.86	68.96	<b>35.70</b>	66.84	85.98	1786.17
+ VTW (K=16)	<b>14.80</b> (51.51%)	<b>65.35</b>	70.00	<b>35.70</b>	<b>67.18</b>	86.33	<b>1857.35</b>

VTW maintain their ability to produce the correct and similar outcomes compared to standard chatbots, despite lacking vision tokens in the deep layers. This highlights VTW’s success in accelerating the chatbot’s responses while holding its performance.

### 4.3 Quantitative Evaluation

#### 4.3.1 Visual Question Answering (VQA)

In the realm of VQA, understanding the image precedes generating an answer, a process facilitated by MLLMs. To assess the efficacy of our VTW, we opt to evaluate on two extensively utilized VQA datasets: AI2D [9] and SQA\_image [8]. As depicted in Table 2, VTW outperforms FastV while consuming fewer FLOPs across three variants of MLLMs. Furthermore, it achieves lossless acceleration compared to the baseline, with nearly half the FLOPs. Notably, VTW even surpasses the baseline in performance, attributed to the mitigation of undesired tokens, particularly in deep layers, where the withdrawal of vision tokens curtails their influence. Table 6 further illustrates how the proposed VTW attains a superior trade-off between performance and accuracy through the utilization of our empirically derived parameter  $K$  with Eq. (6).

#### 4.3.2 Visual Reasoning

Visual reasoning demands heightened perception, knowledge, and reasoning capabilities from the model compared to VQA. We select MMMU\_Val [10] and MMB\_EN [11] datasets for evaluation. The results presented in Table 2 demonstrate that VTW achieves comparable or even superior performance to the baseline and FastV, with fewer FLOPs.

#### 4.3.3 Hallucination Evaluation

Hallucinations can significantly degrade the performance of MLLMs and severely impact user experiences in real-world applications. We conducted experiments on POPE [18] to investigate the impact of VTW on hallucinations. As illustrated in Table 2, VTW achieves comparable performance to the baseline, despite restricting vision tokens to the first few layers of MLLMs. Conversely, FastV, which remove token after the second layer, exacerbates MLLMs’ hallucinations, suggesting that premature removal of vision tokens exacerbates MLLMs hallucinations.

#### 4.3.4 Comprehensive Evaluation

MME [12] is the first comprehensive benchmark for evaluating MLLMs, accessing both perception and cognition across a total of 14 subtasks. To thoroughly gauge the impact of VTW across different tasks, we present the scores for each task in Table 3. VTW demonstrates comparable performance to the baseline across a majority of tasks, including existence, count, color, commonsense reasoning, and artwork. However, VTW exhibits marginal performance degradation on tasks such as position, poster, and OCR. These findings strongly suggest that the information encoded in vision tokens has migrated to subsequent text tokens within the first few layers of MLLMs. To clarify, VTW only involves text tokens in the deep layers of MLLMs. Despite the absence of vision tokens in deep layers, VTW’s performance remains comparable to normal inference, where both vision and text tokens are involved across all layers of MLLMs.



Table 3: Comparison results for the subtasks of MME, including existence, count, position, color, OCR, poster, celebrity, scene, landmark, artwork, commonsense reasoning (Comm.), numerical calculation (Num.), text translation (Text.), and code reasoning (Code.). We utilize **bold** formatting to highlight the best result.

Methods	TFLOPs	Existence	Count	Position	Color	OCR	Poster	Celebrity	Scene	Landmark	Artwork	Comm.	Num.	Text.	Code.	Total
LLaVA-1.5-7B	8.48	<b>190.00</b>	155.00	128.33	170.00	<b>140.00</b>	<b>146.60</b>	137.06	158.00	163.75	119.50	112.86	<b>70.00</b>	107.50	<b>67.50</b>	1866.10
+ FastV	4.91	180.00	155.00	<b>133.33</b>	<b>180.00</b>	137.50	142.52	<b>138.82</b>	<b>160.00</b>	<b>164.50</b>	121.25	116.43	55.00	<b>112.50</b>	67.50	1864.35
+ VTW (K=16)	<b>4.68</b>	<b>190.00</b>	<b>160.00</b>	128.33	170.00	137.50	145.58	135.59	135.59	163.75	<b>123.25</b>	<b>121.43</b>	65.00	115.00	57.50	<b>1872.43</b>
LLaVA-1.5-13B	16.50	<b>185.00</b>	<b>155.00</b>	<b>133.33</b>	170.00	125.00	<b>160.54</b>	152.06	161.25	<b>170.50</b>	<b>118.50</b>	<b>128.57</b>	<b>42.50</b>	77.50	47.50	1827.26
+ FastV	9.56	<b>185.00</b>	<b>155.00</b>	<b>133.33</b>	<b>175.00</b>	<b>132.50</b>	159.52	152.82	<b>161.75</b>	168.25	117.00	126.43	<b>42.50</b>	<b>82.50</b>	<b>57.50</b>	<b>1855.11</b>
+ VTW (K=16)	<b>9.10</b>	<b>185.00</b>	<b>155.00</b>	131.67	<b>175.00</b>	125.00	157.48	<b>153.82</b>	161.25	170.00	<b>118.50</b>	<b>128.57</b>	<b>42.50</b>	77.50	47.50	1828.79
LLaVA-NeXT-7B	28.73	<b>195.00</b>	<b>135.00</b>	<b>143.33</b>	<b>170.00</b>	<b>132.50</b>	<b>159.52</b>	142.94	162.25	155.75	123.25	129.29	<b>42.50</b>	100.00	55.00	1846.33
+ FastV	15.67	<b>195.00</b>	125.00	136.67	<b>170.00</b>	117.50	156.46	140.29	162.25	156.75	123.75	<b>130.00</b>	32.50	87.50	52.50	1786.17
+ VTW (K=16)	<b>14.80</b>	<b>195.00</b>	<b>135.00</b>	133.33	<b>170.00</b>	<b>132.50</b>	<b>159.52</b>	<b>144.71</b>	<b>163.00</b>	<b>158.75</b>	<b>126.25</b>	129.29	<b>42.50</b>	<b>105.00</b>	<b>62.50</b>	<b>1857.35</b>

Table 4: The comparison of GPU memory overhead between VTW and the baseline with KV Cache adopted in inference.

Model	Metric	Baseline	VTW
LLaVA-1.5-7B	(a) Model GPU Memory	14382M	14382M
	(b) Peak GPU Memory during Inference	15372 M	14982 M
	(b) - (a) = Per Sample GPU Memory Overhead	990 M	600 M (0.60 ×)
LLaVA-1.5-13B	(a) Model GPU Memory	27430M	27430M
	(b) Peak GPU Memory during Inference	29022 M	28438 M
	(b) - (a) = Per Sample GPU Memory Overhead	1592 M	1008 M (0.63 ×)
LLaVA-NeXT-7B	(a) Model GPU Memory	14133M	14133M
	(b) Peak GPU Memory during Inference	17189 M	16131M
	(b) - (a) = Per Sample GPU Memory Overhead	3056 M	1998 M (0.65 ×)

## 4.4 Cost Analysis

### 4.4.1 Memory Overhead

The GPU memory overhead comparisons between original MLLMs and our VTW are presented in Table 4. We observe that during the inference of MLLMs, VTW reduces the memory overhead by 35% ~ 40% for each sample. This reduction in memory overhead is substantial, considering that MLLMs typically conduct batch inference in practical scenarios.

### 4.4.2 Flops and Latency

We evaluate the latency of MLLMs on one NVIDIA RTX 3090. For LLaVA-1.5-7B and LLaVA-NeXT-7B, the visual tokens withdrawal layer is manually set to 16, and for LLaVA-1.5-13B, the visual tokens withdrawal layer is set to 20. As depicted in Table 5, VTW reduces FLOPs by nearly half for LLaVA-1.5 and LLaVA-NeXT. The latency of VTW for each sample is approximately 0.64× to 0.77× than that of the baseline models.

Table 5: The comparison of FLOPs and latency between VTW and the baseline on SQA\_Image (2017 examples).

Model	Metric	Baseline	VTW
LLaVA-1.5-7B	TFLOPs	9.3	5.5 (59.14%)
	Total Time (s)	491.0	377.0 (0.77 ×)
	Latency/Example (ms)	243.4	186.9 (0.77 ×)
LLaVA-1.5-13B	TFLOPs	18.2	10.8 (59.34%)
	Total Time (s)	833.0	539.0 (0.65 ×)
	Latency/Example (ms)	413.0	267.2 (0.65 ×)
LLaVA-NeXT-7B	TFLOPs	22.9	12.3 (53.71%)
	Total Time (s)	1050.0	671.0 (0.64 ×)
	Latency/Example (ms)	520.6	332.7 (0.64 ×)

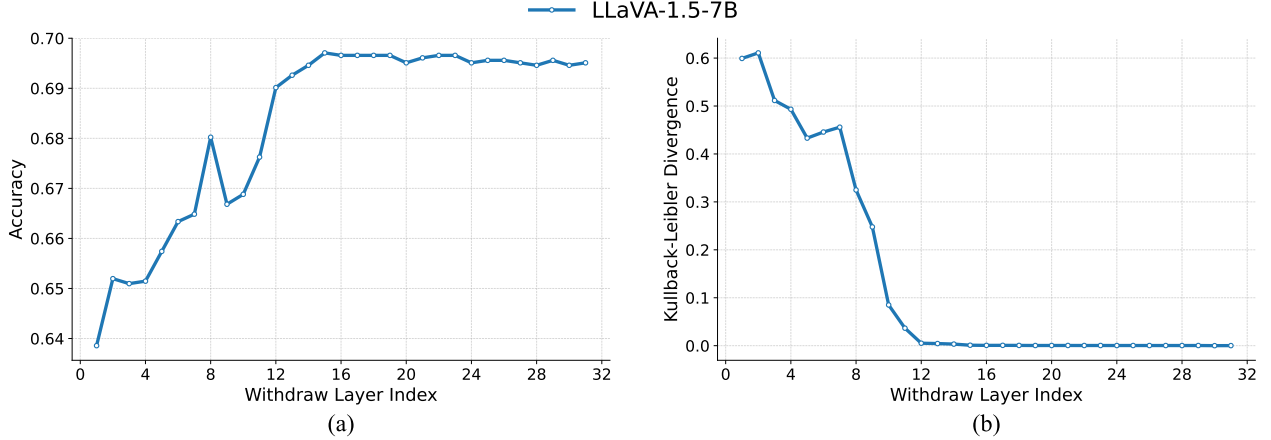


Figure 7: Ablation study on visual tokens withdrawal layer  $K$ . (a) Accuracy v.s.  $K$ ; (b) Kullback-Leibler divergence v.s.  $K$ .

## 4.5 Ablation Studies

We conduct ablation studies using LLaVA-1.5-7B on SQA\_Image.

### 4.5.1 Ablations on Visual Tokens Withdrawal Layers

As depicted in Figure 7(a), a small value of  $K$ , indicating an early withdrawal of vision tokens, leads to a degradation in the performance of MLLMs. When  $K$  exceeds a specific layer number, VTW performs similarly to the baseline. This observation further proves that vision tokens are unnecessary in the deep layers of MLLMs.

Table 6: Ablation study on threshold  $\eta$ .

$\eta$	0.006	0.005	0.004	0.003	0.002	0.001
$K$	12	13	14	15	15	15
Accuracy	69.01	69.26	69.46	69.70	69.70	69.70

### 4.5.2 Ablations on Threshold $\eta$

Recall that we use Kullback-Leibler (KL) divergence as a criterion to determine the withdrawal layer  $K$  on a tiny subset of target datasets, as formulated in Eq. (6). As depicted in Figure 7(b), the KL divergence is large when  $K$  is small, and it converges as  $K$  exceeds a specific threshold. Combining the results from Figure 7(a) and Table 6, we observe that when the KL divergence converges, the accuracy of VTW also converges to that of the baseline. Thus, we select KL as our criterion for determining the withdrawal layer  $K$ , and we set the threshold  $\eta$  in Eq. 6 to 0.003.

Table 7: Ablation study on position embedding. ‘‘Rearrange’’ and ‘‘Keep’’ mean to rearrange and keep the position embeddings of remaining text tokens after withdrawing vision tokens.

Position embedding	SQA_Image	MMMU_Val	POPE
LLaVA-1.5-7B	69.61	35.60	85.83
Rearrange	69.56	35.90	85.41
Keep	<b>69.66</b>	<b>36.30</b>	<b>85.96</b>

### 4.5.3 Ablations on Position Embedding

LLMs use position embeddings to model the positional relationships between tokens. After withdrawing vision tokens, there are two approaches to handle the position embeddings of the remaining text tokens. The first approach is to keep the original position embeddings of the remaining text tokens. The second approach is to rearrange the position

embeddings of the remaining text tokens, indicating that the positions between text tokens are contiguous. As illustrated in Table 7, "Keep" outperforms "Rearrange" in VTW in different datasets.

#### **4.6 Limitations and Future Works**

We present the limitations of our study and outline potential avenues for future research. While our study successfully verifies the phenomenon of information migration within the first few layers of MLLMs, we recognize that more complex tasks may necessitate additional layers to facilitate accurate information migration from vision tokens to subsequent text tokens. Consequently, the reduction in FLOPs is relatively marginal for complex multimodal tasks compared to simpler ones. Due to computational constraints, we did not evaluate the applicability of our VTW in larger models, such as LLaVA-NeXT-34B [6].

Moving forward, future research could explore integrating VTW during the training stage to enhance information migration from vision tokens to subsequent text tokens. This approach has the potential to significantly reduce training and inference cost without compromising the performance of MLLMs. Additionally, there is scope to investigate information migration in other modalities, such as audio and video. Furthermore, we discover that MLLMs can accurately answer some questions based solely on text, which may lead to misinterpretations in the evaluation of MLLMs.

### **5 Conclusion**

In this paper, we introduce visual tokens withdrawal (VTW), a plug-and-play module designed to boost MLLMs for rapid inference. VTW is inspired by two intriguing phenomena observed in MLLMs: (1) The attention sink phenomenon in LLMs persists in MLLMs. (2) The occurrence of information migration, indicating that visual information migrates to subsequent text tokens within the first few layers of MLLMs. Building upon these observations, we deduce that vision tokens become unnecessary in the deep layers of MLLMs, despite they take up a significant computational overhead. Thus, we strategically withdraw vision tokens at specific layers in MLLMs. Experiments across various multimodal tasks and chatbot scenarios validate the efficacy of VTW in boosting MLLMs for rapid inference without compromising performance.

### **6 Acknowledgement**

This work was supported by National Science and Technology Major Project (No. 2022ZD0118201), the National Science Fund for Distinguished Young Scholars (No.62025603), the National Natural Science Foundation of China (No. U21B2037, No. U22B2051, No. 62176222, No. 62176223, No. 62176226, No. 62072386, No. 62072387, No. 62072389, No. 62002305 and No. 62272401), and the Natural Science Foundation of Fujian Province of China (No.2021J01002, No.2022J06001).

## References

- [1] Josh Achiam, Steven Adler, Sandhini Agarwal, Lama Ahmad, Ilge Akkaya, Florencia Leoni Aleman, Diogo Almeida, Janko Altenschmidt, Sam Altman, Shyamal Anadkat, et al. Gpt-4 technical report, 2023.
- [2] Gemini Team, Rohan Anil, Sebastian Borgeaud, Yonghui Wu, Jean-Baptiste Alayrac, Jiahui Yu, Radu Soricut, Johan Schalkwyk, Andrew M Dai, Anja Hauth, et al. Gemini: A family of highly capable multimodal models, 2023.
- [3] Hugo Touvron, Thibaut Lavril, Gautier Izacard, Xavier Martinet, Marie-Anne Lachaux, Timothée Lacroix, Baptiste Rozière, Naman Goyal, Eric Hambro, Faisal Azhar, et al. Llama: Open and efficient foundation language models, 2023.
- [4] Haotian Liu, Chunyuan Li, Qingyang Wu, and Yong Jae Lee. Visual instruction tuning. In *NeurIPS*, pages 1–19, 2023.
- [5] Junnan Li, Dongxu Li, Silvio Savarese, and Steven Hoi. Blip-2: Bootstrapping language-image pre-training with frozen image encoders and large language models. In *ICML*, pages 19730–19742, 2023.
- [6] Haotian Liu, Chunyuan Li, Yuheng Li, Bo Li, Yuanhan Zhang, Sheng Shen, and Yong Jae Lee. Llava-next: Improved reasoning, ocr, and world knowledge, January 2024.
- [7] Alec Radford, Jong Wook Kim, Chris Hallacy, Aditya Ramesh, Gabriel Goh, Sandhini Agarwal, Girish Sastry, Amanda Askell, Pamela Mishkin, Jack Clark, Gretchen Krueger, and Ilya Sutskever. Learning transferable visual models from natural language supervision. In *ICML*, pages 8748–8763, 2021.
- [8] Pan Lu, Swaroop Mishra, Tanglin Xia, Liang Qiu, Kai-Wei Chang, Song-Chun Zhu, Oyvind Tafjord, Peter Clark, and Ashwin Kalyan. Learn to explain: Multimodal reasoning via thought chains for science question answering. In *NeurIPS*, pages 2507–2521, 2022.
- [9] Aniruddha Kembhavi, Mike Salvato, Eric Kolve, Minjoon Seo, Hannaneh Hajishirzi, and Ali Farhadi. A diagram is worth a dozen images. In *ECCV*, pages 235–251, 2016.
- [10] Xiang Yue, Yuansheng Ni, Kai Zhang, Tianyu Zheng, Ruoqi Liu, Ge Zhang, Samuel Stevens, Dongfu Jiang, Weiming Ren, Yuxuan Sun, et al. Mmmu: A massive multi-discipline multimodal understanding and reasoning benchmark for expert agi, 2023.
- [11] Yuan Liu, Haodong Duan, Yuanhan Zhang, Bo Li, Songyang Zhang, Wangbo Zhao, Yike Yuan, Jiaqi Wang, Conghui He, Ziwei Liu, et al. Mmbench: Is your multi-modal model an all-around player?, 2023.
- [12] Chaoyou Fu, Peixian Chen, Yunhang Shen, Yulei Qin, Mengdan Zhang, Xu Lin, Jinrui Yang, Xiawu Zheng, Ke Li, Xing Sun, Yunsheng Wu, and Rongrong Ji. Mme: A comprehensive evaluation benchmark for multimodal large language models, 2023.
- [13] Reiner Pope, Sholto Douglas, Aakanksha Chowdhery, Jacob Devlin, James Bradbury, Jonathan Heek, Kefan Xiao, Shivani Agrawal, and Jeff Dean. Efficiently scaling transformer inference. In *MLsys*, pages 1–18, 2023.
- [14] Liang Chen, Haozhe Zhao, Tianyu Liu, Shuai Bai, Junyang Lin, Chang Zhou, and Baobao Chang. An image is worth 1/2 tokens after layer 2: Plug-and-play inference acceleration for large vision-language models, 2024.
- [15] Dachuan Shi, Chaofan Tao, Anyi Rao, Zhendong Yang, Chun Yuan, and Jiaqi Wang. Crossget: Cross-guided ensemble of tokens for accelerating vision-language transformers, 2023.
- [16] Jianjian Cao, Peng Ye, Shengze Li, Chong Yu, Yansong Tang, Jiwen Lu, and Tao Chen. Madtp: Multimodal alignment-guided dynamic token pruning for accelerating vision-language transformer, 2024.
- [17] Yuzhang Shang, Mu Cai, Bingxin Xu, Yong Jae Lee, and Yan Yan. Llava-prumerge: Adaptive token reduction for efficient large multimodal models, 2024.
- [18] Yifan Li, Yifan Du, Kun Zhou, Jinpeng Wang, Wayne Xin Zhao, and Ji-Rong Wen. Evaluating object hallucination in large vision-language models, 2023.
- [19] Guangxuan Xiao, Yuandong Tian, Beidi Chen, Song Han, and Mike Lewis. Efficient streaming language models with attention sinks, 2023.
- [20] Long Ouyang, Jeffrey Wu, Xu Jiang, Diogo Almeida, Carroll Wainwright, Pamela Mishkin, Chong Zhang, Sandhini Agarwal, Katarina Slama, Alex Ray, John Schulman, Jacob Hilton, Fraser Kelton, Luke Miller, Maddie Simens, Amanda Askell, Peter Welinder, Paul F Christiano, Jan Leike, and Ryan Lowe. Training language models to follow instructions with human feedback. In *NeurIPS*, pages 27730–27744, 2022.
- [21] Hugo Touvron, Louis Martin, Kevin Stone, Peter Albert, Amjad Almahairi, Yasmine Babaei, Nikolay Bashlykov, Soumya Batra, Prajjwal Bhargava, Shrubti Bhosale, et al. Llama 2: Open foundation and fine-tuned chat models, 2023.

- [22] Deyao Zhu, Jun Chen, Xiaoqian Shen, Xiang Li, and Mohamed Elhoseiny. Minigpt-4: Enhancing vision-language understanding with advanced large language models, 2023.
- [23] Hang Zhang, Xin Li, and Lidong Bing. Video-llama: An instruction-tuned audio-visual language model for video understanding, 2023.
- [24] Dong Zhang, Shimin Li, Xin Zhang, Jun Zhan, Pengyu Wang, Yaqian Zhou, and Xipeng Qiu. Speechgpt: Empowering large language models with intrinsic cross-modal conversational abilities, 2023.
- [25] Haotian Liu, Chunyuan Li, Yuheng Li, and Yong Jae Lee. Improved baselines with visual instruction tuning, 2023.
- [26] Bin Lin, Bin Zhu, Yang Ye, Munan Ning, Peng Jin, and Li Yuan. Video-llava: Learning united visual representation by alignment before projection, 2023.
- [27] Yongming Rao, Wenliang Zhao, Benlin Liu, Jiwen Lu, Jie Zhou, and Cho-Jui Hsieh. Dynamicvit: Efficient vision transformers with dynamic token sparsification. In *NeurIPS*, pages 13937–13949, 2021.
- [28] Yifan Xu, Zhijie Zhang, Mengdan Zhang, Kekai Sheng, Ke Li, Weiming Dong, Liqing Zhang, Changsheng Xu, and Xing Sun. Evo-vit: Slow-fast token evolution for dynamic vision transformer. In *AAAI*, pages 2964–2972, 2022.
- [29] Youwei Liang, GE Chongjian, Zhan Tong, Yibing Song, Jue Wang, and Pengtao Xie. Evit: Expediting vision transformers via token reorganizations. In *ICLR*, pages 1–21, 2022.
- [30] Daniel Bolya, Cheng-Yang Fu, Xiaoliang Dai, Peizhao Zhang, Christoph Feichtenhofer, and Judy Hoffman. Token merging: Your vit but faster. In *ICLR*, pages 1–20, 2023.
- [31] Dmitrii Marin, Jen-Hao Rick Chang, Anurag Ranjan, Anish Prabhu, Mohammad Rastegari, and Oncel Tuzel. Token pooling in vision transformers, 2021.
- [32] Alexey Dosovitskiy, Lucas Beyer, Alexander Kolesnikov, Dirk Weissenborn, Xiaohua Zhai, Thomas Unterthiner, Mostafa Dehghani, Matthias Minderer, Georg Heigold, Sylvain Gelly, et al. An image is worth 16x16 words: Transformers for image recognition at scale. In *ICLR*, pages 1–22, 2021.
- [33] Mengzhao Chen, Wenqi Shao, Peng Xu, Mingbao Lin, Kaipeng Zhang, Fei Chao, Rongrong Ji, Yu Qiao, and Ping Luo. Diffrate : Differentiable compression rate for efficient vision transformers. In *ICCV*, pages 17164–17174, 2023.
- [34] Xinjian Wu, Fanhu Zeng, Xiudong Wang, Yunhe Wang, and Xinghao Chen. Ppt: Token pruning and pooling for efficient vision transformers, 2023.
- [35] Saurabh Goyal, Anamitra Roy Choudhury, Saurabh Raje, Venkatesan Chakaravarthy, Yogish Sabharwal, and Ashish Verma. Power-bert: Accelerating bert inference via progressive word-vector elimination. In *ICML*, pages 3690–3699, 2020.
- [36] Sehoon Kim, Sheng Shen, David Thorsley, Amir Gholami, Woosuk Kwon, Joseph Hassoun, and Kurt Keutzer. Learned token pruning for transformers. In *KDD*, pages 784–794, 2022.
- [37] Wei-Lin Chiang, Zhuohan Li, Zi Lin, Ying Sheng, Zhanghao Wu, Hao Zhang, Lianmin Zheng, Siyuan Zhuang, Yonghao Zhuang, Joseph E. Gonzalez, Ion Stoica, and Eric P. Xing. Vicuna: An open-source chatbot impressing gpt-4 with 90%\* chatgpt quality, March 2023.
- [38] Mengzhao Chen, Mingbao Lin, Ke Li, Yunhang Shen, Yongjian Wu, Fei Chao, and Rongrong Ji. Cf-vit: A general coarse-to-fine method for vision transformer. In *AAAI*, pages 7042–7052, 2023.
- [39] Weihang Wang, Qingsong Lv, Wenmeng Yu, Wenyi Hong, Ji Qi, Yan Wang, Junhui Ji, Zhuoyi Yang, Lei Zhao, Xixuan Song, Jiazheng Xu, Bin Xu, Juanzi Li, Yuxiao Dong, Ming Ding, and Jie Tang. Cogvlm: Visual expert for pretrained language models, 2023.
- [40] Alex Young, Bei Chen, Chao Li, Chengen Huang, Ge Zhang, Guanwei Zhang, Heng Li, Jiangcheng Zhu, Jianqun Chen, Jing Chang, et al. Yi: Open foundation models by 01. ai, 2024.
- [41] Kaichen Zhang Bo Li, Peiyuan Zhang et al. Lmms-eval: Accelerating the development of large multimodal models, March 2024.

## A More Multimodal Chatbot Results

More multimodal chatbot dialogues are provided in Figure 8, Figure 9, and Figure 10. We withdraw vision tokens at the 16-th, 16-th, and 20-th layers for LLaVA-1.5-7B [4], LLaVA-NeXT-7B [6], and LLaVA-1.5-13B [4], respectively. Our VTW significantly reduces FLOPs by over 40% for multimodal chatbots, while maintaining the quality of responses. As shown in Figure 8, Figure 9, and Figure 10, the chatbots with our VTW are comparable to standard decoding in different multimodal tasks, such as VQA (answering the color of the truck and the gender of the driver), image caption (describing the detail of image), OCR (recognizing the logo of the car), and vision reasoning (reasoning the service of the car and the time of day).

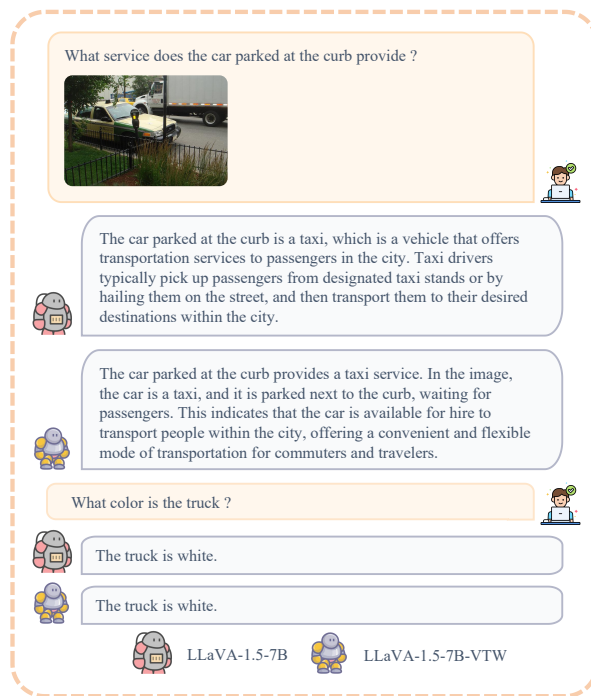


Figure 8: The chatbot dialogue comparison between original LLaVA-1.5-7B [4] and our LLaVA-1.5-7B-VTW.

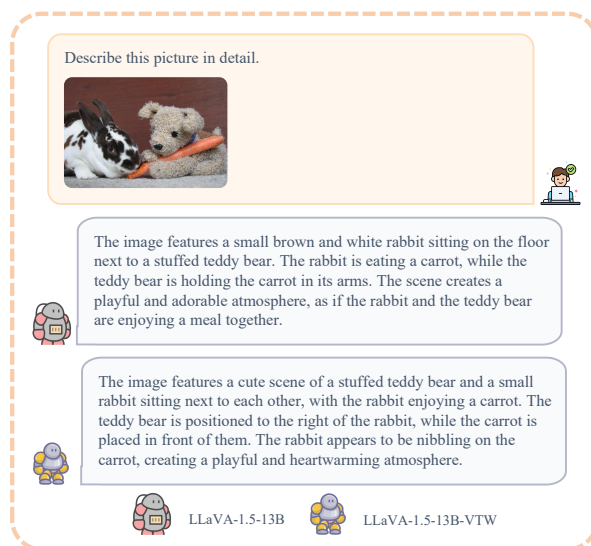



Figure 9: The chatbot dialogue comparison between original LLaVA-1.5-13B [4] and our LLaVA-1.5-13B-VTW.

What time of day is it ?



It's difficult to determine the exact time of day from the image alone, but it appears to be daytime. The lighting suggests it's not too dark, and there are no visible signs of artificial lighting that would indicate it's nighttime.

It's difficult to determine the exact time of day from the image alone, but it appears to be daylight, as the shadows are not very pronounced. The sky is not completely dark, which suggests it's not nighttime.

Is the driver a man or a woman ?

The driver of the car in the image is a man.

The driver in the image is a man.

What company does a taxi belong to ?

The taxi in the image belongs to a company called "ComCab."

The taxi in the image belongs to ComCab, as indicated by the logo on the side of the vehicle.

LLaVA-NeXT-7B      LLaVA-NeXT-7B-VTW

Figure 10: The chatbot dialogue comparison between original LLaVA-NeXT-7B [6] and our LLaVA-NeXT-7B-VTW.